

DOI: 10.1002/adem.200900281

Tensile Deformation Behaviors of Cu–Ni Alloy Processed by Equal Channel Angular Pressing**

By Jiangwei Wang, Peng Zhang, Qiqiang Duan, Gang Yang, Shiding Wu and Zhefeng Zhang*

The microstructure of the Cu–Ni alloy specimen ER is mainly elongated coarse grains. However, the microstructure of the specimen EH is inhomogeneous and some recrystallized sub-grains form. In addition, the misorientation angles of the specimens ER and EH are mainly smaller than 15° , showing a feature of low-angle grain boundaries. Although the uniform elongation of the ECAPed Cu–Ni alloy decreases rapidly, the yield strength of the Cu–Ni alloy is improved more than three times after ECAP for one pass. The mechanical properties, deformation, and fracture of Cu–Ni alloy are not significantly affected by the strain rates. With the increase in strain rates, the yield strength of the specimen E0 hardly changes but the ultimate tensile strength increases slightly. However, with the increase in strain rates, the tensile strength of the specimen EH gradually improved. Besides, the fracture fractographies of the specimens EH turn into shear dimples at high strain rate. In addition, both the strain-hardening exponent n and strain-rate sensitivity m of the specimens EH are small, inducing lower strain-hardening, uniform plastic deformation and resistance to the shear deformation.

Copper and its alloys are widely used in industry. In the past few years, high-performance Cu alloys have been investigated extensively.^[1–5] The copper alloys which have the main alloying element of nickel are called cupronickel alloy or white brass.^[1] Due to the excellent properties, such as high electron properties, high strength, and excellent corrosion resistance to the sea water, Cu–Ni alloy has been widely used in industry.^[1–5] Recently, how to prepare high-

performance Cu–Ni based alloys has attracted much attention.^[1–4]

In the past decade, the technique of equal channel angular pressing (ECAP) has drawn much attention as a method of severe plastic deformation (SPD) to improve the mechanical properties of materials.^[6–8] Up to now, many metals and alloys, which have high strength or superplasticity, have been fabricated via ECAP technique, albeit their ductility is decreased in comparison with that of their coarse-grained counterparts.^[6,7] Recently, high-performance Cu alloys produced by ECAP technique have attracted more and more attention. Some Cu alloys with high-performance have been fabricated by ECAP and their properties have been investigated, such as the superplasticity of Cu–Zn alloy, the ferromagnetic performance of Cu–Co alloy, microstructure of Cu–Si alloy, and mechanical properties of Cu–Cr and Cu–Cr–Zr alloys.^[9–13] Moreover, Cu–Zn and Cu–Al alloys with high strength and certain ductility, produced by SPD, have also been studied.^[14–16] However, compared with pure Al and its alloys, the research of SPD Cu alloys is only confined to just a few kinds of alloys.^[6,9–16] Hence, how to expand the research to other Cu alloys should be conducted in the future. In the present work, the Cu–Ni alloy was processed by ECAP to investigate its tensile deformation behaviors and mechanical properties at room temperature (RT) and different strain rates. Because it is the first time to process Cu–Ni alloy by ECAP, we primarily compare its tensile properties after one-pass pressing at different strain rates.

[*] Prof. Z. F. Zhang, Dr. J. W. Wang, Dr. P. Zhang,
Dr. Q. Q. Duan, Prof. S. D. Wu
Shenyang National Laboratory for Materials Science, Institute
of Metal Research, Chinese Academy of Sciences 72 Wenhua
Road, Shenyang 110016, PR China
E-mail: zhfzhang@imr.ac.cn
Prof. G. Yang
Central Iron and Steel Research Institute
Beijing 100081, PR China

[**] The authors would like to thank Mrs. W. Gao, Mrs. M. J. Zhang for their help of EBSD analysis, SEM observations, and stimulating discussions, and Dr. F. Yang for checking the english. This work is supported by National Natural Science Foundation of China (NSFC) under grant no. 50890173. Z. F. Zhang would like to acknowledge the financial support of "Hundred of Talents Project" by Chinese Academy of Sciences and the National Outstanding Young Scientist Foundation under grant no. 50625103.

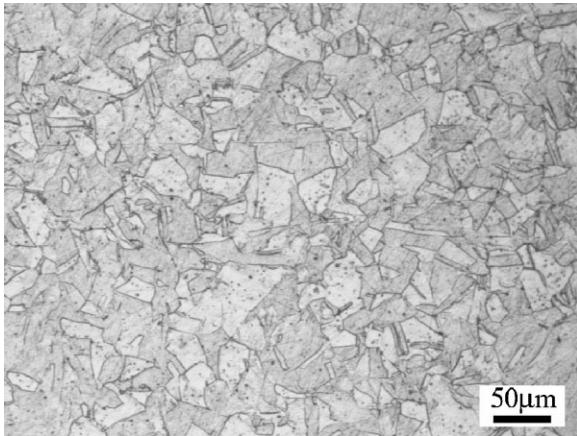


Fig. 1. The microstructure of the Cu–Ni alloy annealed at 840 °C for 1.5 h.

Experimental

The experimental material in present work is Cu-40 wt% Ni-1.5 wt% Mn alloy. The Cu–Ni alloy bars were annealed in vacuum furnace at 840 °C for 1.5 h, gaining the average grain size of about 45 μm with some annealed twins inside the grains (Fig. 1). The alloy bars were made into some billets with a dimension of $\Phi 8 \text{ mm} \times 45 \text{ mm}$. Then, ECAP was conducted at RT and high temperature, respectively, using the die whose channel angle is $\Phi = 90^\circ$ and $\Psi = 30^\circ$. When extruded at high temperature, the specimens were preserved at 350 °C for

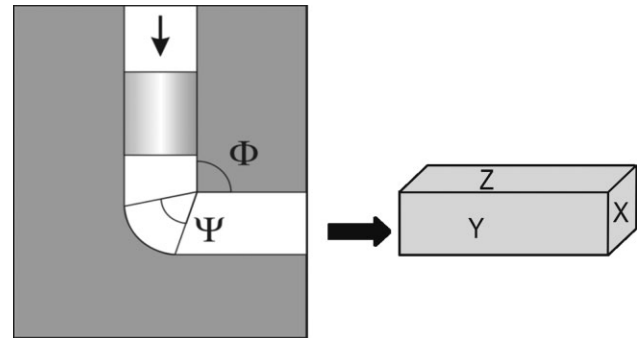


Fig. 2. Illustration of the ECAP die and three directions.

10 min and then pressed through the die. Hereafter, the annealed specimens are labeled as E0, and the specimens conducted at RT and high temperature are defined as ER and EH, respectively. Three separate orthogonal planes are also defined in Figure 2 where these planes are the X or transverse plane perpendicular to the flow direction, the Y or flow plane parallel to the side face at the point of exit from the die and the Z or longitudinal plane parallel to the top surface at the point of exit from the die, respectively^[6]. In addition, because of the rapid strain hardening of the Cu–Ni alloy, the pressing was conducted only for one pass.

After ECAP, the specimens for electron backscatter diffraction (EBSD) observations were cut from the center of the ECAPed bars parallel to the Y plane. After mechanically

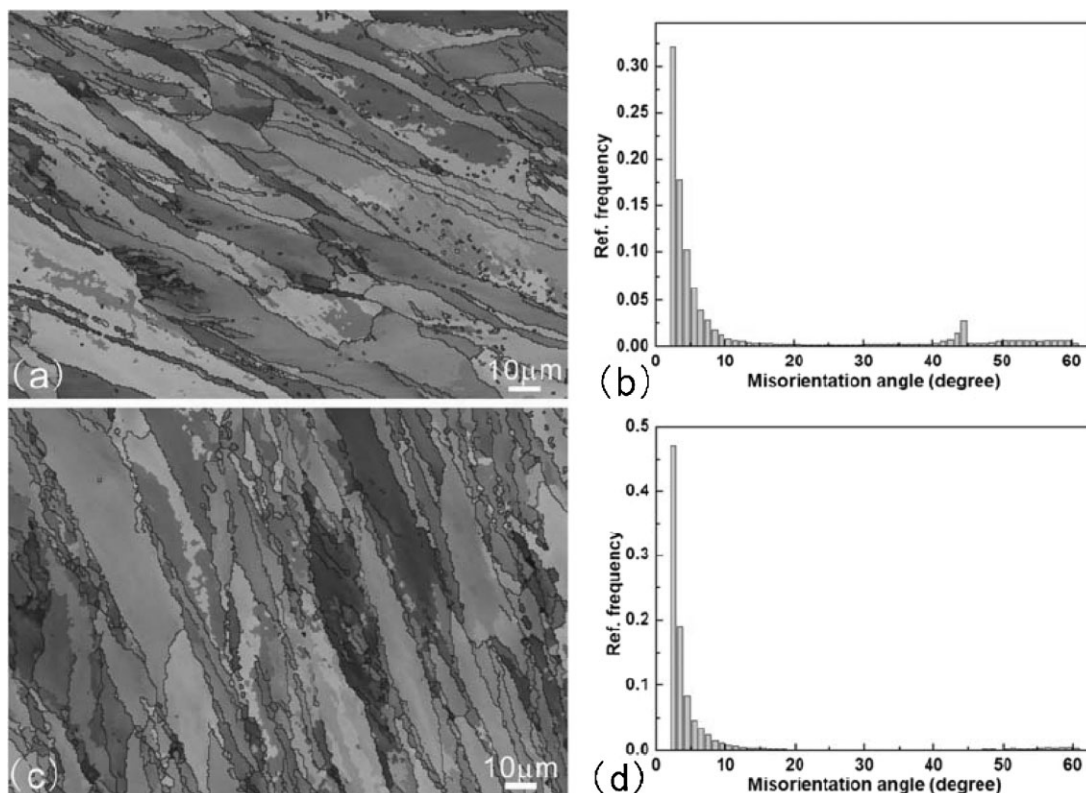


Fig. 3. EBSD micrographies and misorientation for the specimens ER and EH (Y plane). (a, b) ER; (c, d) EH.

ground and polished, some EBSD samples with a diameter of 3 mm were punched for ion milling at -40°C , 2 h. Then, the samples were observed by LEO Supra 35 scanning electron microscope (SEM) equipped with an EBSD system.

The tensile specimens with cross-section of $1.5\text{ mm} \times 2\text{ mm}$ and gauge length of 8 mm were machined from the annealed and ECAPed samples, with their tensile axes parallel to the extrusion direction. And then, the tensile specimens were mechanically ground and finally mechanically polished. Tensile experiments were conducted at RT using the Instron 8871 testing machine operated at a constant cross-head speed with a strain rate of about $5 \times 10^{-4}\text{ s}^{-1}$. Furthermore, to understand the deformation behaviors of Cu–Ni alloy comprehensively, tensile tests were also conducted at different strain rates ranging from 5×10^{-4} to $1 \times 10^{-1}\text{ s}^{-1}$ in the specimens E0 and EH. Besides, three to five tensile experiments were conducted to check the repeatability of the results up to fracture. Because it is difficult to press more Cu–Ni alloy bars at RT, the specimens ER were not performed at different strain rates. After the tensile tests, surface deformation morphologies and fractographies were observed using a LEO Supra 35 SEM and the Vickers hardness tests were conducted by using the MVK-H3 hardness-testing device.

Results

Figure 3 is the EBSD micrographies and misorientation for the samples ER and EH. It is apparent that the microstructure of the specimen ER is mainly the elongated coarse grains [Fig. 3(a)]. The grain boundaries of the specimens ER are found to be mainly low-angle ones, because most of them have misorientations less than 15° [Fig. 3(b)]. However, there are also some high-angle grain boundaries between 40° and 50° . On the contrary, the distribution of grains in the specimen EH is inhomogeneous [Fig. 3(c)]. In some zones, dynamic recovery or dynamic recrystallization occurs and relatively small grains or sub-grains form; whereas, there are also some coarse grains in other zones, which are just elongated along the ECAP shear direction. In addition, there are primarily low-angle grain boundaries and the high-angle ones almost disappear in the specimen EH [Fig. 3(d)].

The tensile stress–strain curves of the Cu–Ni alloy are shown in Figure 4(a), which were conducted at RT with a constant strain rate of $5 \times 10^{-4}\text{ s}^{-1}$. Their mechanical properties are listed in Table 1. Apparently, the strength of the ECAPed specimens is enhanced and the ductility decreases dramatically. The yield strength (YS) of the Cu–Ni alloy increases from 134 MPa of the specimen E0 to higher than 546 MPa even after only one-pass ECAP. Meanwhile, the ultimate tensile strength (UTS) improves from 389 MPa of the specimen E0 to higher than 568 MPa after ECAP. Nevertheless, similar to most of the ECAPed materials, the uniform elongation (UE) of the ECAPed Cu–Ni alloy decreases rapidly, from 44% of the specimen E0 to lower than 5% after ECAP, inducing low resistance to the necking. The hardness of

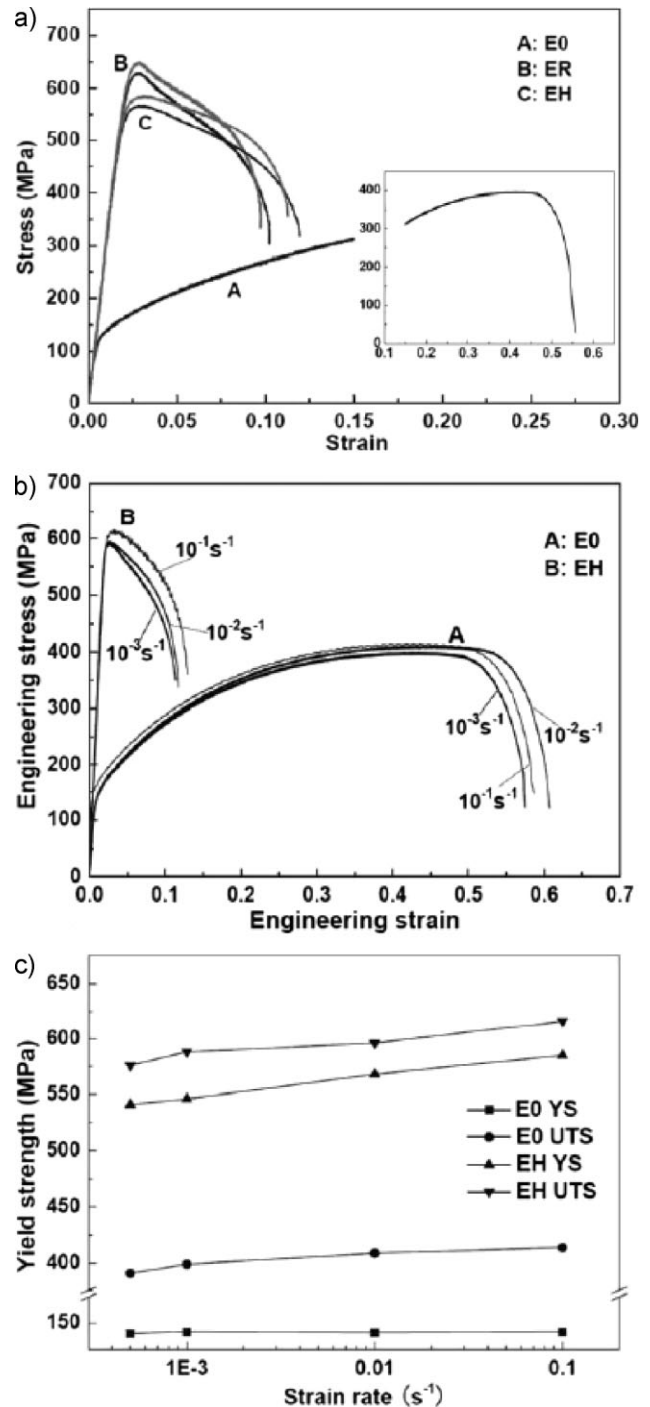


Fig. 4. (a) The tensile engineering (black) and true (red) stress–strain curves of the Cu–Ni alloys before and after ECAP; (b) the tensile stress–strain curves of the specimens E0 and EH at different strain rates; (c) the dependence of YS and UTS on the strain rates of the specimens E0 and EH.

Table 1. Strength, UE, and hardness of the Cu–Ni alloy specimens before and after ECAP.

Specimens	E0	EH	ER
σ_b [MPa]	389	568	629
$\sigma_{0.2}$ [MPa]	134	546	591
UE [%]	44	3.4	2.8
HV [MPa]	125	203	213

the Cu–Ni alloy is also shown in Table 1. It can be seen that the change of hardness is closely associated with the strength, increasing from HV125 of the specimen E0 to more than HV200 after ECAP.

When pressed at different temperatures, the mechanical properties of the specimens are slightly different. From Figure 4(a) and Table 1, it can be seen that the strength of the specimen EH is lower than that of the specimen ER; however, the elongation of the specimen EH is slightly higher than that of the specimen ER.

The tensile engineering stress–strain curves of the specimens E0 and EH at different strain rates are shown in Figure 4(b). It can be seen that the stress–strain curves of Cu–Ni alloy are not affected apparently by the strain rates. Figure 4(c) demonstrates the dependence of strength on the strain rates. The YS of the specimens E0 hardly changes with the strain rates; whereas, the UTS of the specimens E0 increases gradually with the strain rates. On the contrary, both YS and UTS of the specimens EH increase with the strain rates. Moreover, the ductility of the specimens EH is improved slightly at higher strain rate [Fig. 4(b)].

The surface deformation morphologies of the tensile specimens are shown in Figure 5, which were conducted at the strain rate of $5 \times 10^{-4} \text{ s}^{-1}$. In the specimens E0, surface plastic deformation occurred on the whole gauge part of the tensile specimens and there is apparent necking near the fracture zone. Meanwhile, many slip bands arise on the surface of the specimens E0, most of which are confined in the interior of the coarse grains [Fig. 5(a)]. In addition, there are also some deformation morphologies, showing the crossing of slip bands through some twin boundaries [Fig. 5(b)]. For the specimens EH, their deformation morphologies are shown in Figure 5(c). It is found that the plastic deformation of the specimens EH mainly concentrates near the necking zone. In addition, there are some dense shear bands on the surface of the specimens EH [Fig. 5(c)], which is different from that of the specimens E0. Most of the shear bands can continuously cross through the grain boundaries and link with each other. Because the microstructure of the specimens EH is inhomogeneous, some coarse grains with dense shear bands can also be seen. Besides, the plastic deformation behaviors of the specimens ER are similar to that of the specimens EH, which is not shown here.

Moreover, the surface fracture morphologies of the specimens E0 and ER are also various at different strain rates. Figure 6 presents the surface fracture morphologies of the specimens E0 and ER at different strain rates. The fracture morphologies of the specimen E0 are similar at all strain rates, with obvious necking near the fracture zone [Fig. 6(a) and (b)]. Different from that of the specimens E0, the specimens EH show some features of shear fracture at all the strain rates [Fig. 6(c) and (d)]. The fracture angles of the specimens EH are 53° at $1 \times 10^{-3} \text{ s}^{-1}$ and 60° at $1 \times 10^{-1} \text{ s}^{-1}$, respectively. This indicates that the shear stress plays an important role in the fracture of the specimens EH. Besides, all the fracture angles arise on the Y plane of the ECAPed specimens. In some other

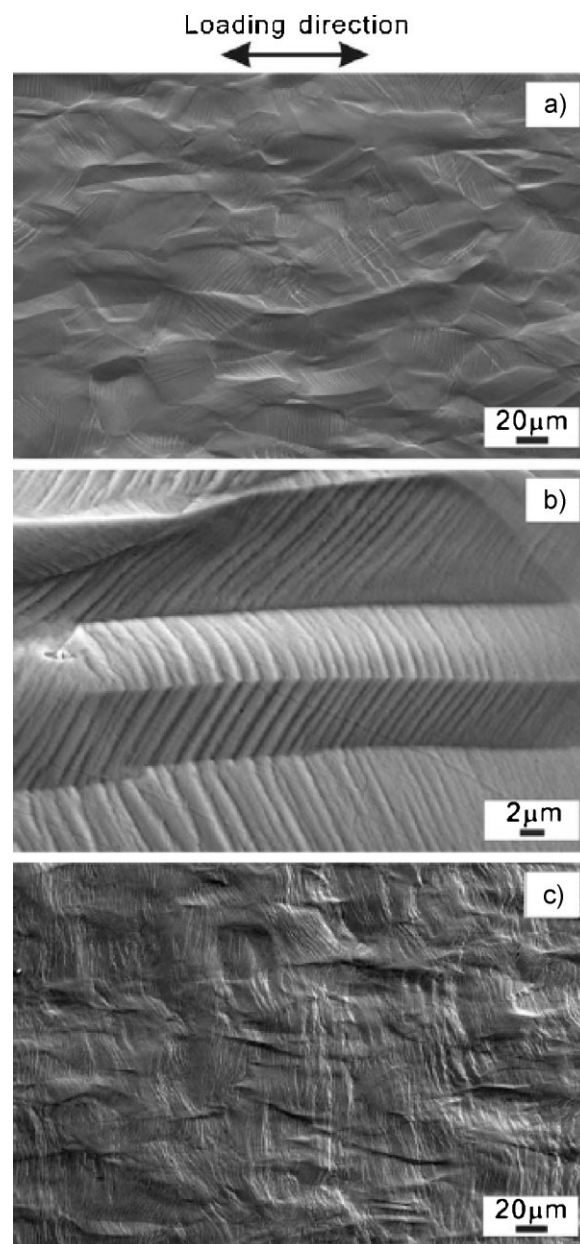


Fig. 5. Tensile surface deformation morphologies of the Cu–Ni alloy before and after ECAP. (a) and (b) E0; (c) EH (Z plane).

ECAPed materials, such as Al–Mg alloy and the specimens ER, the fracture angle also arises on the Y plane of ECAPed materials.^[17,18] It means that the shear deformation during ECAP has some impact on the deformation and fracture behaviors of the ECAPed materials.

With the increase in strain rate, the tensile fractographies of the specimens E0 and EH also have some changes. Figure 7 is the fractographies of the specimens E0, which are similar at different strain rates. All of the specimens E0 have some shear lips near the edge of the fracture zone, as well as the equiaxial dimples in the center of the fracture zone, as presented in Figure 7. On the contrary, the specimens EH show different fracture characteristics (Fig. 8). At low strain rate, it is primarily equiaxial dimples, which homogeneously distribute

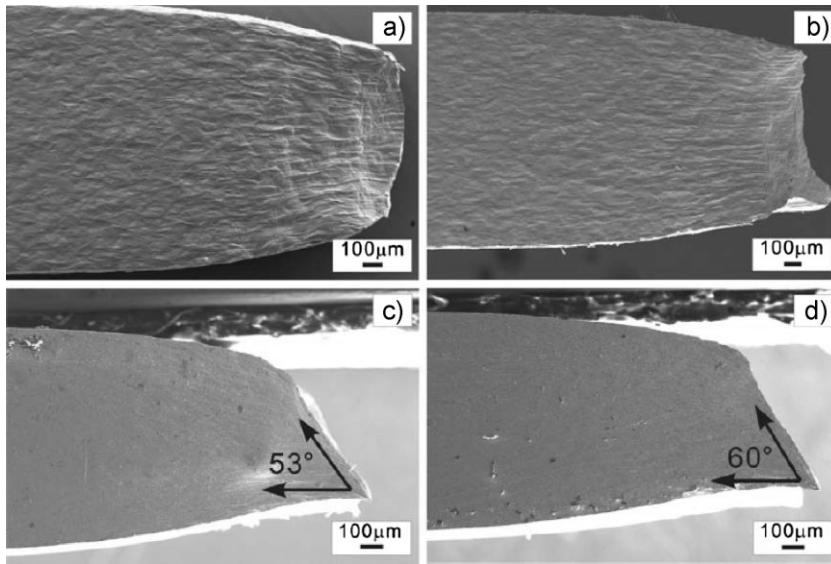


Fig. 6. Tensile fracture morphologies of the specimens E0 at strain rate of (a) $1 \times 10^{-3} \text{ s}^{-1}$ and (b) $1 \times 10^{-1} \text{ s}^{-1}$; tensile fracture morphologies of the specimens EH (Y plane) at strain rate of (c) $1 \times 10^{-3} \text{ s}^{-1}$ and (d) $1 \times 10^{-1} \text{ s}^{-1}$.

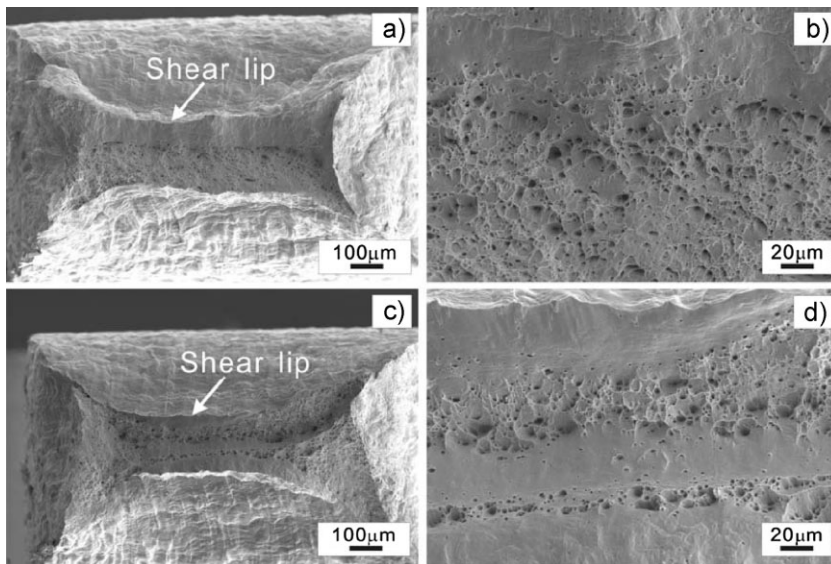


Fig. 7. The tensile fractographies of the specimens E0 at different strain rates. (a, b) $1 \times 10^{-3} \text{ s}^{-1}$; (c, d) $1 \times 10^{-1} \text{ s}^{-1}$.

in the center of the fracture zone. At the edge of the fracture zone, some shear lips arise [Fig. 8(a)]. Whereas, at high strain rate, it is mainly separated shear dimples in the fracture zone and the shear lips disappear [Fig. 8(c) and (d)]. The elongated direction of shear dimples is along the shear direction [Fig. 8(d)]. The shear dimples also indicate that shear deformation becomes the primary deformation mechanism for the specimens EH.

Discussion

Microstructure and Properties of Specimens EH

Generally, the misorientation angles between grain boundaries in completely recrystallized materials are primarily

high-angle ones.^[19] However, because the temperature of ECAP extrusion is low and the processing time of specimens EH through ECAP die is short, the dynamic recovery or recrystallization is incomplete. This will induce partial recovery or annihilation of dislocations, leading to the formation of some sub-grains with low-angle grain boundaries in some zones [Fig. 3(c) and (d)], whose misorientation angles between grain boundaries are usually lower than 15° .^[19] Besides, partial recovery or annihilation of dislocations also means lower dislocation density in the specimen EH. During the following tensile deformation of specimen EH, more dislocations can also be accommodated before necking, inducing the slightly higher ductility and relatively lower strength [Fig. 4(a) and Table 1].

Strain-Hardening Behavior

In the tensile true stress–strain curves, the relationship between flow stress and strain in the stage of uniform plastic deformation can be expressed as^[20,21]

$$\sigma_T = K(\epsilon_T)^n \tag{1}$$

where σ_T is the true stress, ϵ_T is the true strain, n is the strain-hardening exponent, and K is the strength coefficient. This equation is called as Hollomon relationship.^[20,21] The strain-hardening exponent n reflects the ability of resistance to plastic deformation of materials,^[20,21] that is, the higher strain-hardening exponent n means the higher resistance to plastic deformation and necking.^[21] The strain-hardening exponent n can be obtained by the following equation:

$$\lg \sigma_T = \lg K + n \lg \epsilon_T \tag{2}$$

By using Equation (2), the strain-hardening exponent n of the specimen E0 was calculated to be 0.390. However, because of the low uniform plasticity of the ECAPed specimens, if its strain-hardening exponent n is determined by Equation (2), there will be a big error.

In addition to Equation (2), there is another method to simply gain the strain-hardening exponent n of materials, which can be expressed as^[20]

$$\epsilon_\mu = n \tag{3}$$

where ϵ_u is the true UE, and the strain-hardening exponent n is equal to ϵ_u .^[20] By using Equation (3), the values n of Cu–Ni alloy were measured, as listed in Table 2. The value n of the specimen E0 is about 0.378, which is approximately equal to the calculated value by using Equation (2). The values n of the

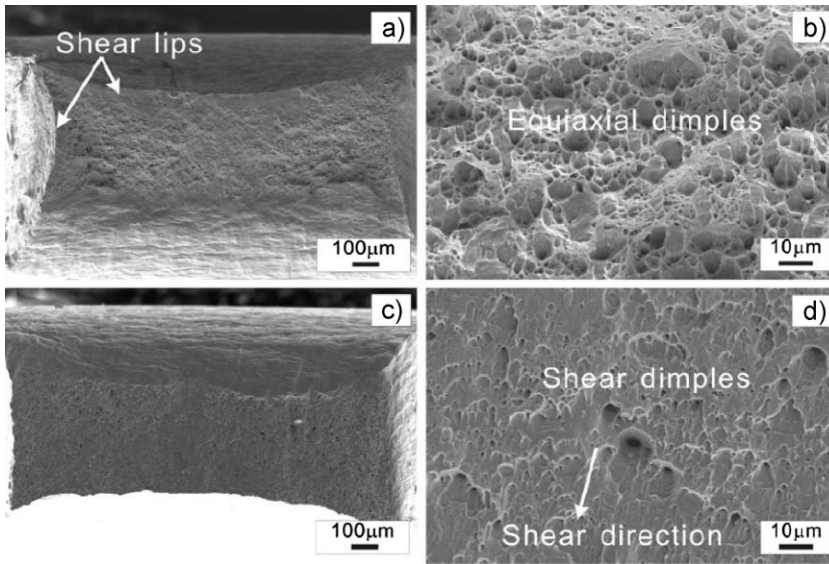


Fig. 8. The tensile fractographies of the specimens ER at different strain rates. (a, b) $1 \times 10^{-3} \text{ s}^{-1}$; (c, d) $1 \times 10^{-1} \text{ s}^{-1}$.

specimens EH and ER were measured to be 0.035 and 0.029, respectively. It can be seen that the value n of the specimen EH is slightly higher than that of the specimen ER, which might be induced by the dynamic recovery during ECAP at high temperature. The higher strain-hardening exponent n means better abilities of strain-hardening and resistance to plastic deformation and necking.^[21,22]

In addition, according to the Considère criterion, non-uniform deformation occurs when the following condition is reached:^[22,23]

$$\left(\frac{\partial \sigma}{\partial \varepsilon}\right)_{\dot{\varepsilon}} \leq \sigma \quad (4)$$

where σ and ε are the true stress and true strain, respectively, and $\dot{\varepsilon}$ is the strain rate. The left-hand term represents the strain-hardening rate. It means that the necking occurs when the strain-hardening rate exceeds the true stress at constant strain rate.^[22,23] For the ECAPed Cu–Ni alloy, its strength is extremely high [right-hand term of Eq. (4)] and its strain-hardening rate is low [left-hand term of Eq. (4)], making it easy onset for the inhomogeneous deformation at small strain. The lower value n of the ECAPed Cu–Ni alloy also illustrates this point, which means the occurrence of necking after very little strain-hardening and uniform plastic deformation. In order to improve the UE of the ECAPed Cu–Ni alloy, one method is to further process the samples at high temperature for

Table 2. Strain-hardening exponent n of the Cu–Ni alloys before and after ECAP.

Specimens	E0	EH	ER
n	0.390	—	—
$n(\dot{\varepsilon}_a)$	0.378	0.035	0.029

multiple passes; another is to adjust its microstructures through subsequent heat-treatment after ECAP.

Strain-Rate Sensitivity

Strain rate plays important roles in the deformation mechanism and mechanical properties of metallic materials. Generally, the flow stress of materials increases with the increase in strain rates, which is called as strain-rate hardening.^[20,21] The change of strength with strain rates can be expressed by strain-rate sensitivity m .^[20,21] Moreover increase in the strain rates could also promote the strain-hardening ability to some extent, which could enhance the UE and the total tensile strain.^[22,23] Hence, the higher strain-rate sensitivity m not only means the higher strain-rate hardening ability but also a higher resistance to necking during tension and superplastic deformation ability at proper temperature.^[20–23] The relationship

between strain-rate sensitivity m and flow stress can be expressed as^[20,21]

$$\sigma = K \dot{\varepsilon}^m \quad (5)$$

In the above equation, $\dot{\varepsilon}$ is the strain rate, K is the flow stress of materials at the unit strain rate, which is a constant of materials. The above relationship can also be expressed as^[20]

$$m = \left. \frac{\partial \ln \sigma}{\partial \ln \dot{\varepsilon}} \right|_{\varepsilon, T} \quad (6)$$

By using Equation (6), the strain-rate sensitivity m can be calculated.

For the specimens E0 and EH, the dependence in flow stresses on the strain rates is shown in Figure 9. It can be seen that the flow stresses of the specimens E0 and EH increase

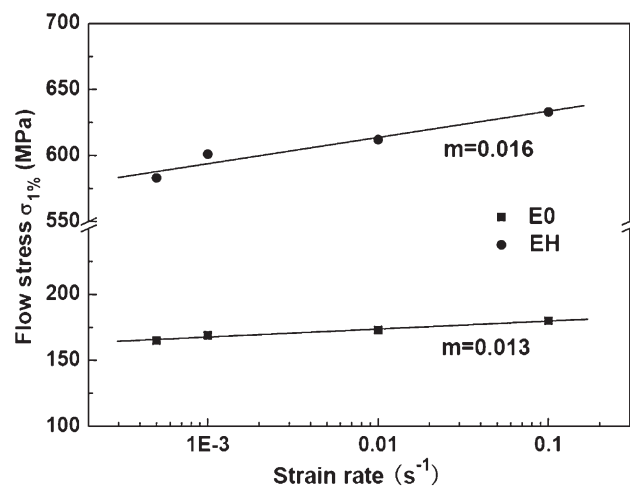


Fig. 9. The dependence of flow stress on the tensile strain rates of the specimens E0 and EH.

slightly with increase in the strain rates. Besides, it should be noted that both the specimens E0 and EH have a small strain-rate sensitivity m in the strain rate range from 5×10^{-4} to 10^{-1} s^{-1} , which is 0.013 for E0 and 0.016 for EH. It means that both the specimens E0 and EH display lower dependence of flow stress on the strain rates, and show a slight strain-rate hardening ability (Fig. 9). Generally, the m value of bcc metals decreases rapidly with refining their grain size down to the nanoscale.^[22] On the contrary, the strain-rate sensitivity m of fcc metals increases gradually with the decrease in the grain size.^[22] For the coarse-grained Cu, m is 0.011, as well as 0.036 for the electrodeposited nanoscale Cu, 0.015 for the ECAPed ultra-fine grained (UFG) Cu and 0.03–0.04 for the Cryo-rolled UFG Cu.^[23–25]

The strain-hardening exponent n and strain-rate sensitivity m play important roles in the plastic deformation of materials.^[20–23] For the materials sensitive to the strain-rate, the presence of the strain-rate sensitivity of the flow stress, m , helps to sustain the uniform deformation.^[22,23] Hence, m must be considered in the unstable criterion. According to the Hart instability criterion^[22,23,26]

$$\frac{1}{\sigma} \left(\frac{\partial \sigma}{\partial \epsilon} \right)_\epsilon - 1 + m \leq 0 \quad (7)$$

for the high-strength materials, sufficiently large strain-hardening ability, and/or strain-rate hardening needs to be present to sustain the uniform straining before the onset of localized deformation.^[22,23,26] For the specimens E0, though m is low, n is sufficiently high, which means that the strain-hardening rate is large and more homogeneous deformation can be contained before necking. On the contrary, both n and m of the ECAPed Cu–Ni alloys are still lower and inadequate to stabilize the large uniform tensile deformation. This explains why localized deformation or necking always occurs in the metals produced by SPD as soon as the diminishing strain-hardening can no longer compete with the shrinkage in the cross-sectional area.^[23] Besides, the lower m also indicates insufficient resistance to the shear deformation, inducing the shear deformation as the primary plastic deformation mechanism.^[23] Therefore, it is necessary to further consider the shear deformation and the fracture features.

Deformation Mechanism and Shear Dimple

Dimple is the typical fracture morphology of ductile materials.^[20,21] The shape of dimples changes with the stress condition: the dimples are equiaxial under normal stress; whereas, the dimples will extend along the shear direction to form shear or elongated ones under shear stress.

During the tensile test, the voids will be preferential to nucleate in the zone with high strain concentration, and then grow, coalesce, and link with each other, eventually induce fracture. There are many factors, such as the strength of matrix, influencing the voids nucleation.^[27] Generally, the void nucleation occurs at lower plastic strain in the high-strength ones for the identical material.^[27] For the specimens E0, its strength is low and the voids will nucleate at high

plastic strain, showing a higher UE (Fig. 4 and Table 1). For the specimens EH, the voids will nucleate at lower plastic strain and induce necking. On the other hand, the deformation mechanism also changes after ECAP. The specimens E0 display ductile fracture controlled by the normal stress, as seen in Figure 6(a) and (b). After ECAP, the deformation mechanism has changed into shear fracture and shear deformation becomes the dominating deformation mechanism, which can be seen from Figure 6(c) and (d). Fang *et al.* investigated the deformation and fracture of the ECAPed Al-2.77 wt% Mg alloy.^[18] Similar to the specimen EH, this alloy has a fracture angle of 50° on Y plane after one-pass ECAP. It was suggested that the shear fracture of the Al-2.77 wt% Mg alloy was controlled by both shear and normal stresses during tensile deformation.^[18]

Furthermore, strain rate also plays an important role in the deformation behaviors of materials.^[20–26] With the increase of strain rates, the shape of dimples in the fracture zone of the specimens EH changes from equiaxial to shear dimples (Fig. 8). Figure 10 illustrates the formation processes of the equiaxial and shear dimples. Under low strain rate, the voids have enough time to expand along the cross direction after nucleation, and link with each other to form the equiaxial dimples, as illustrated in Figure 10(a). However, during plastic deformation, the relative deformation rate is enhanced when increasing the strain rate. When the strain rate exceeds the limitation, such as $1 \times 10^{-1} \text{ s}^{-1}$, it will restrict the plastic deformation and induce extremely uneven plastic deformation. As a result, the deformation resistance of materials is enhanced, which can be seen from Figure 9. Meanwhile, it will also trigger the shear deformation at high strain rate in the materials with a lower m .^[23] Even at ductile fracture, the concentration mechanism of voids will be rapidly transformed to shear fracture at high strain rate and form severe shear bands between voids, as illustrated in Figure 10(b). The shear deformation will induce the dimples shearing, elongating

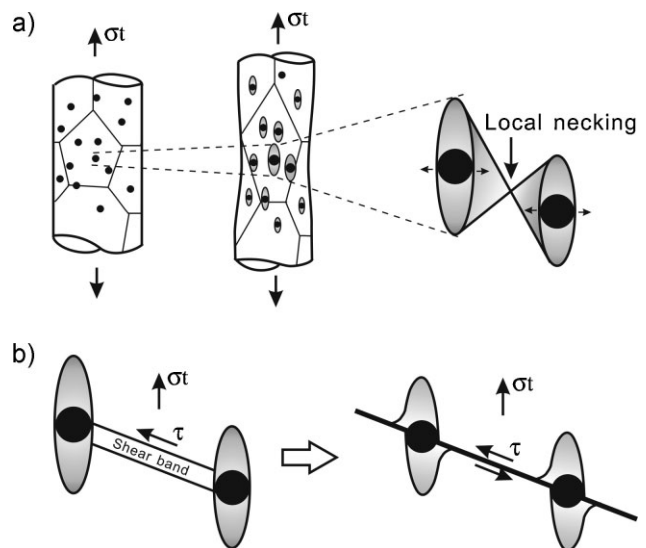


Fig. 10. Illustration of the formation process of dimples. (a) Equiaxial dimple; (b) shear dimple.

along the shear stress direction and resulting in the shear dimples eventually, as demonstrated in Figure 8(d) and 10(b).

Received: October 19, 2009

Final Version: January 16, 2010

-
- [1] J. W. Martin, *Mater. Eng.* **2006**, 94.
- [2] R. Nowosielski, P. Sakiewicz, P. Gramatyka, *J. Mater. Proc. Technol.* **2005**, 162, 379.
- [3] S. Suzuki, N. Shibusani, K. Mimura, M. Isshiki, Y. Waseda, *J. Alloys Compd.* **2006**, 417, 116.
- [4] S. Han, K. Sohn, C. Kim, S. Kim, *Metall. Mater. Trans. A* **2004**, 35, 465.
- [5] M. A. Al-Thubaitia, T. Hodgkiessb, S. Y. K. Ho, *Desalination* **2005**, 183, 195.
- [6] R. Z. Valiev, T. G. Langdon, *Prog. Mater. Sci.* **2006**, 51, 881.
- [7] M. Furukawa, Z. Horita, T. G. Langdon, *Adv. Eng. Mater.* **2001**, 3, 121.
- [8] W. Z. Han, Z. F. Zhang, S. D. Wu, S. X. Li, *Acta Mater.* **2007**, 55, 5889.
- [9] K. Neishi, Z. Horita, T. G. Langdon, *Scr. Mater.* **2001**, 45, 333.
- [10] T. Fujita, S. Nishimura, T. Fujinami, K. Kaneko, Z. Horita, D. J. Smith, *Mater. Sci. Eng. A* **2006**, 417, 149.
- [11] W. Z. Han, Z. F. Zhang, S. D. Wu, C. X. Huang, S. X. Li, *Adv. Eng. Mater.* **2008**, 10, 1110.
- [12] A. Vinogradov, V. Patlan, Y. Suzuki, K. Kitagawa, V. I. Kopylov, *Acta Mater.* **2002**, 50, 1639.
- [13] C. Z. Xu, Q. J. Wang, M. S. Zheng, J. W. Zhu, J. D. Li, M. Q. Huang, Q. M. Jia, Z. Z. Du, *Mater. Sci. Eng. A* **2007**, 459, 303.
- [14] Y. H. Zhao, Y. T. Zhu, X. Z. Liao, Z. Horita, T. G. Langdon, *Appl. Phys. Lett.* **2006**, 89, 121906.
- [15] X. H. An, W. Z. Han, C. X. Huang, P. Zhang, G. Yang, S. D. Wu, Z. F. Zhang, *Appl. Phys. Lett.* **2008**, 92, 201915.
- [16] S. Qu, X. H. An, H. J. Yang, C. X. Huang, G. Yang, Q. S. Zang, Z. G. Wang, Z. F. Zhang, *Acta Mater.* **2009**, 57, 1586.
- [17] D. R. Fang, Z. F. Zhang, S. D. Wu, C. X. Huang, H. Zhang, N. Q. Zhao, J. J. Li, *Mater. Sci. Eng. A* **2006**, 426, 305.
- [18] D. R. Fang, Q. Q. Duan, N. Q. Zhao, J. J. Li, S. D. Wu, Z. F. Zhang, *Mater. Sci. Eng. A* **2007**, 459, 137.
- [19] F. J. Humphreys, *J. Mater. Sci.* **2001**, 36, 3833.
- [20] M. A. Meyers, K. K. Chawla, *Mech. Behav. Mater.* **1999**, 115.
- [21] T. H. Courtney, *Mech. Behav. Mater.* **2000**, 13–16, 509.
- [22] Y. M. Wang, E. Ma, *Acta Mater.* **2004**, 52, 1699.
- [23] Y. M. Wang, E. Ma, *Mater. Sci. Eng. A* **2004**, 375, 46.
- [24] L. Lu, S. X. Li, K. Lu, *Scr. Mater.* **2001**, 45, 1163.
- [25] G. T. Gray, T. C. Lowe, C. M. Cady, R. Z. Valiev, I. V. Aleksandrov, *Nanostruct. Mater.* **1997**, 9, 477.
- [26] E. W. Hart, *Acta Metall.* **1967**, 15, 351.
- [27] W. M. Garrison, Jr, N. R. Moody, *J. Phys. Chem. Solids* **1987**, 48, 1035.
-